Supplemental Table 1. Endpoints reached for the MEL270 efficacy study.

Group	ID	Activity (kBq)	Experimental Endpoint	Clinical Endpoint				Notes (d p.i. = days post injection, t.v. tumor volume at clinical endpoint, mets = metastases)
			Size of Tumor >2000 mm^3	Weight Loss	Sick*	Tumor Ulceration	Death	
Saline	1	NA	X					112 d p.i., mets in lung.
	2	NA	X					91 d p.i.
	3	NA	X					124 d p.i., mets in liver and lung, enlarged spleen and thyroid.
	4	NA			X			96 d p.i., 1346 mm^3 t.v.
	5	NA			X			109 d p.i., mets in liver, enlarged spleen, 1597 mm^3 t.v.
	6	NA			X			112 d p.i., 956 mm^3 t.v.
	7	NA			X			125 d p.i., 1212mm^3 t.v.
	8	NA	X					75 d p.i.
	9	NA			X			125 d p.i., 962 mm3 t.v., mets in lung, enlarged thyroid.
	10	NA	X					112 d p.i.
	11	NA			X			112 d p.i., 1358 mm^3 t.v.
La-DOTA-MC1RL	12	NA			X			88 d p.i., 978 mm^3 t.v.
	13	NA	X					119 d p.i.
	14	NA	X					68 d p.i.
	15	NA	X					102 d p.i.
	16	NA	X					102 d p.i.
	17	NA	X					124 d p.i., mets in liver and lung, enlarged thyroid.
	18	NA	X					109 d p.i.
	19	NA			X			125 d p.i., 717 mm^3 t.v.
	20	NA		X	X			88 d p.i., 996 mm^3 t.v.
	21	NA	X					109 d p.i., mets in lungs.
	22	NA	X					88 d p.i.
^{225}Ac-DOTA-SP	23	93.24		X				25 d p.i., 36 mm^3 t.v.
	24	140.23		X				58 d p.i., 493 mm^3 t.v.
	25	77.70					X	102 d p.i., 613 mm^3 t.v.
	26	61.79			X	X		78 d p.i., 1108 mm^3 t.v., mets in liver.
	27	36.63		X	X			124 d p.i., 990 mm^3 t.v.
	28	128.02		X	X			58 d p.i., 40 mm^3 t.v.
	29	76.96			X			112 d p.i., 287 mm^3 t.v., mets in liver.
	30	143.93		X	X			119 d p.i., 522 mm^3 t.v.
	31	120.25		X				35 d p.i., 26 mm^3 t.v.
	32	112.11		X	X			119 d p.i., 888 mm^3 t.v.
	33	117.66		X				35 d p.i., 32 mm^3 t.v.
^{225}Ac-DOTA-MC1RL	34	113.59		X				158 d p.i., 476 mm^3 t.v.
	35	85.10	X					168 d p.i., mets in liver.
	36	112.48		X	X			130 d p.i., 482 mm^3 t.v.
	37	112.85	X					158 d p.i.
	38	93.24	X					130 d p.i., mets in liver, enlarged spleen.
	39	46.62		X				119 d p.i., 307 mm^3 t.v.
	40	83.99		X				124 d p.i., 554 mm^3 t.v.
	41	98.42		X				154 d p.i., mets in lung, tumor volume at euthanasia: 717 mm^3
	42	95.83				X		158 d p.i., 792 mm^3 t.v., mets in liver.
	43	79.18	X					168 d p.i.
	44	104.71	X					161 d p.i.

*Sick animals exhibited: Hunched back, decreased grooming, lethargy, rapidly declining condition or moribund appearance, and were euthanized after consultation with Veterinary staff.

NA= Not Applicable

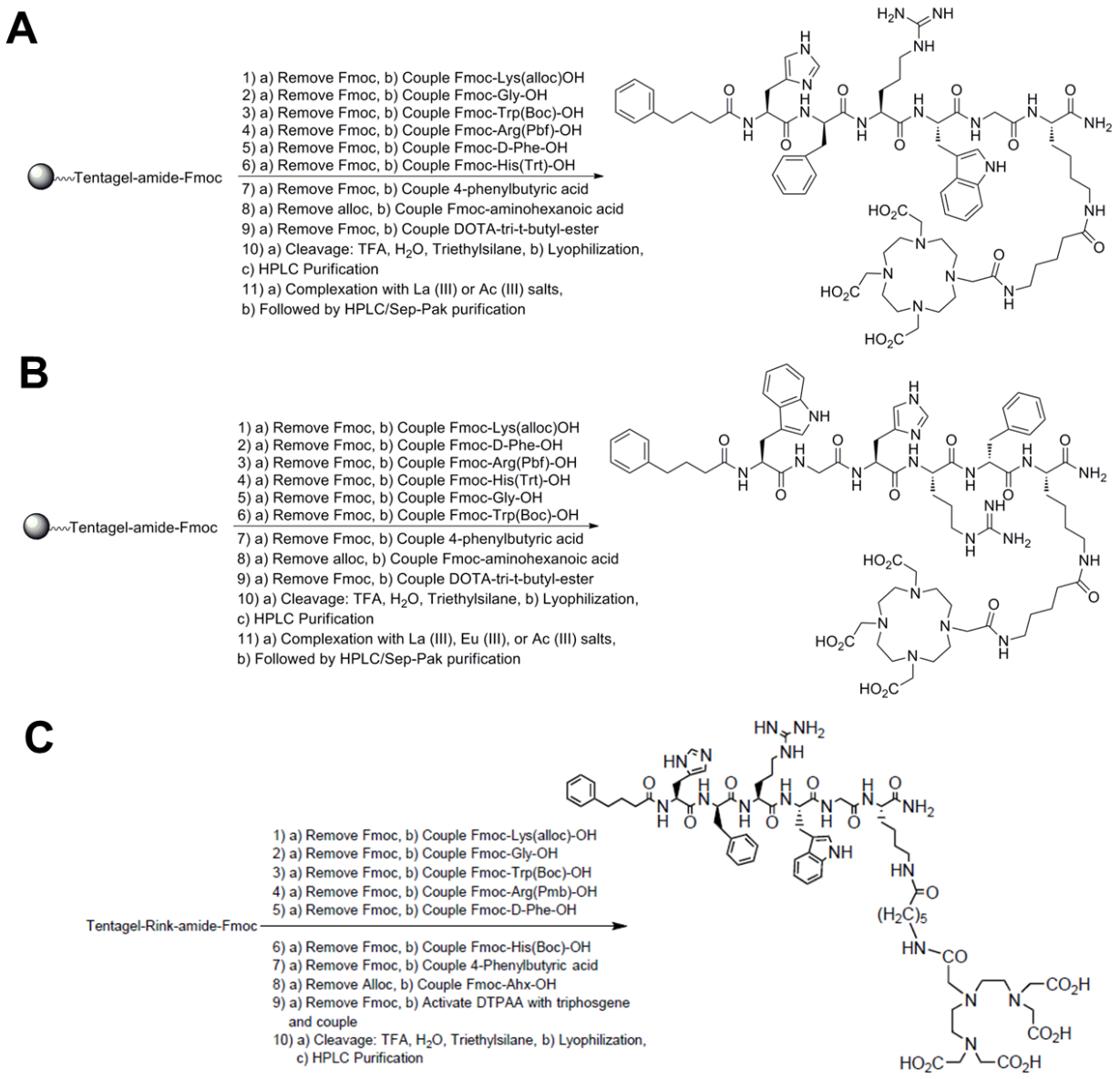

Supplemental Figure 1. Scheme showing synthetic route to metal chelation. (A) DOTA-MC1RL,(B) DOTA-SP and (C) Eu-DTPA-MC1RL. Metal chelated structures are not shown.

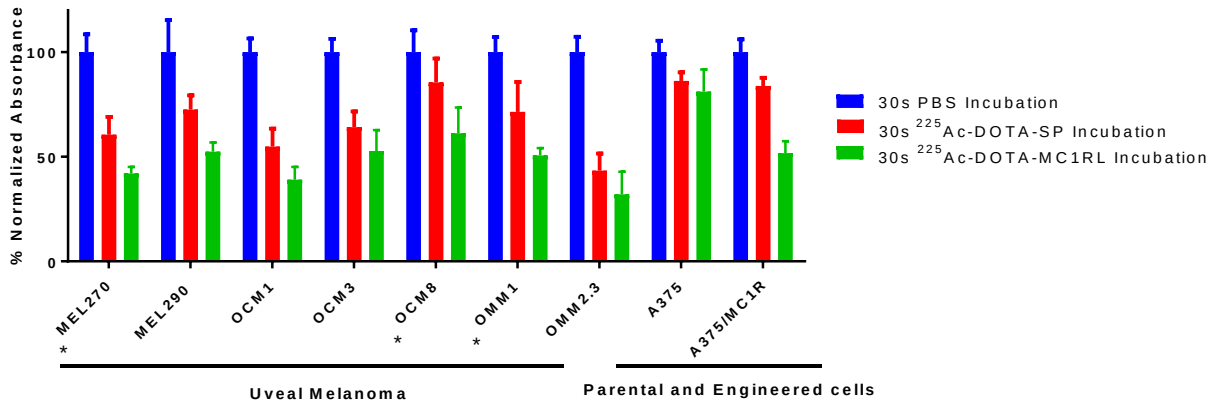

Supplemental Figure 2. MC1R-specific cytotoxicity results for cell lines. Cells were plated at a density of 10,000-15,000 cells/well (96 well plate, n=8 wells per cell line) for 24 h. Medium was aspirated and 20 µl containing 10.7 kBq of ^{225}Ac-DOTA-MC1RL or ^{225}Ac-DOTA-SP activity in PBS were added to each well. After 30 seconds, the plates were washed 3X with PBS and culture media replaced. After 48 h incubation at 5% CO_2 and 37°C, a CCK-8 colorimetric cell proliferation/cytotoxicity assay (Dojindo) was performed and absorbance measured using a Multiskan plate reader (ThermoFischer). Activities were determined using the AtomLab 500 Dose Calibrator (BioDex) and the 38.2 energy dial number. The PBS incubation control values were used for normalization. Data were first analyzed for normality using the Anderson-Darling statistic then Analysis of Variance (ANOVA) was used to determine differences among the groups. The Bonferroni-Holm correction for multiple testing was used to adjust the p-values. The Ryan-Einot-Gabriel-Welsch Multiple Range Test was used, controlling the familywise error rate at α=0.05, for pairwise comparisons between the control, scrambled and targeted cohorts within each cell line.

*Cells with the GNAQ or GNA11 uveal melanoma mutations.

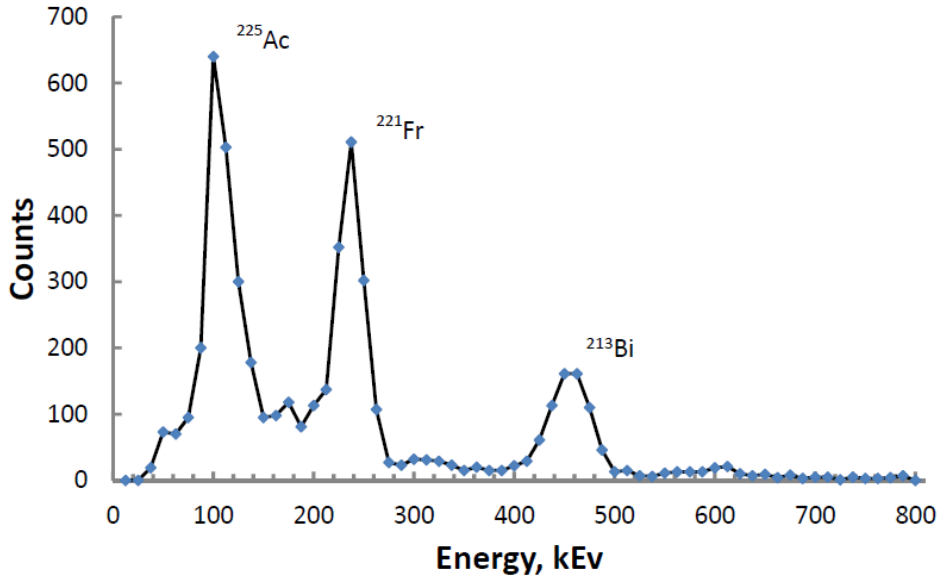

Supplemental Figure 3. Gamma spectrum of ^{225}Ac and the ^{221}Fr and ^{213}Bi decay products. The BioDex Atom Lab 500 Gamma Wipe Test Counter was used to generate this spectrum from a sample containing ^{225}Ac-DOTA-MC1RL.

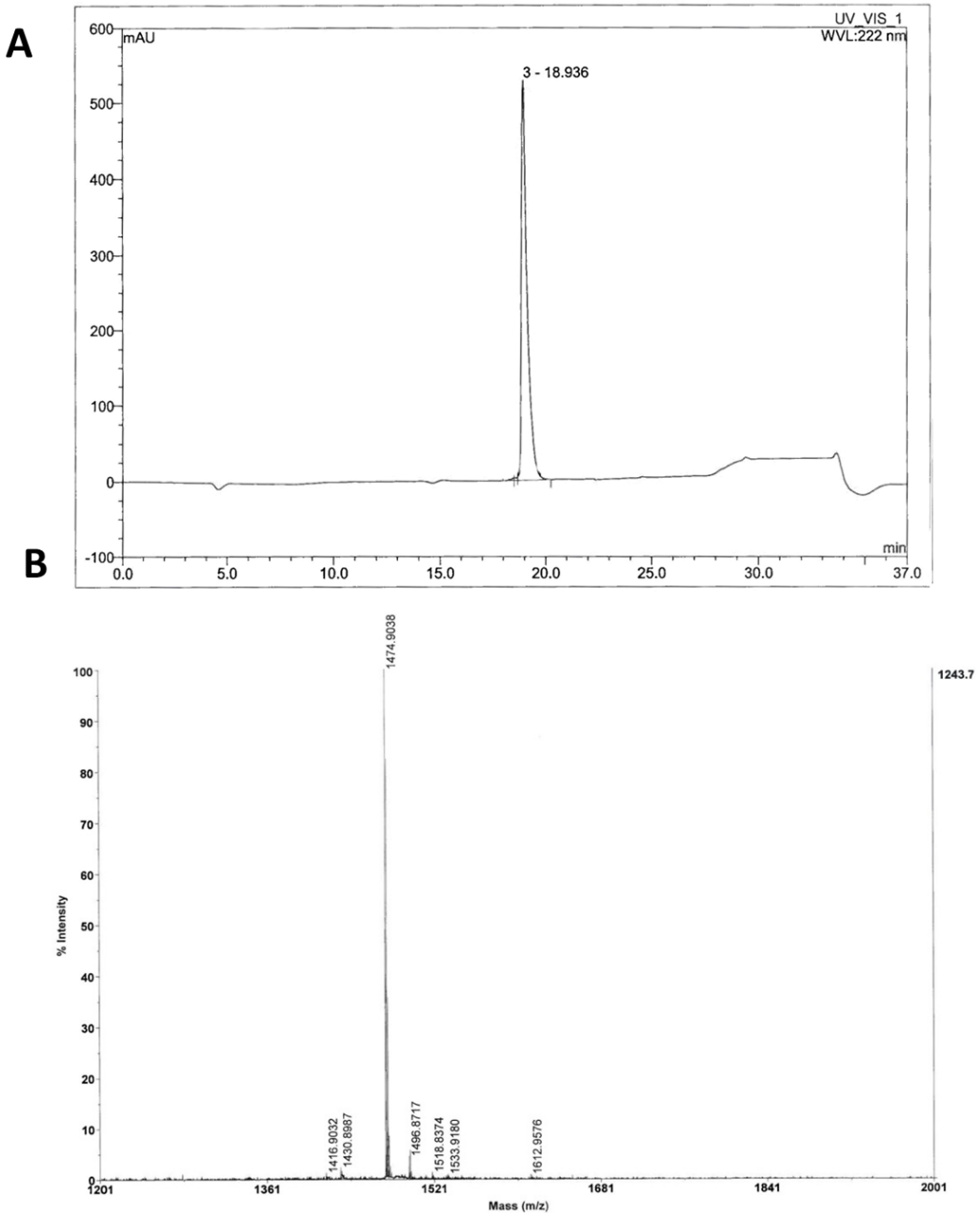

Supplemental Figure 4. (A) Analytical HPLC chromatogram and (B) MALDI-TOF of DOTA-MC1RL.

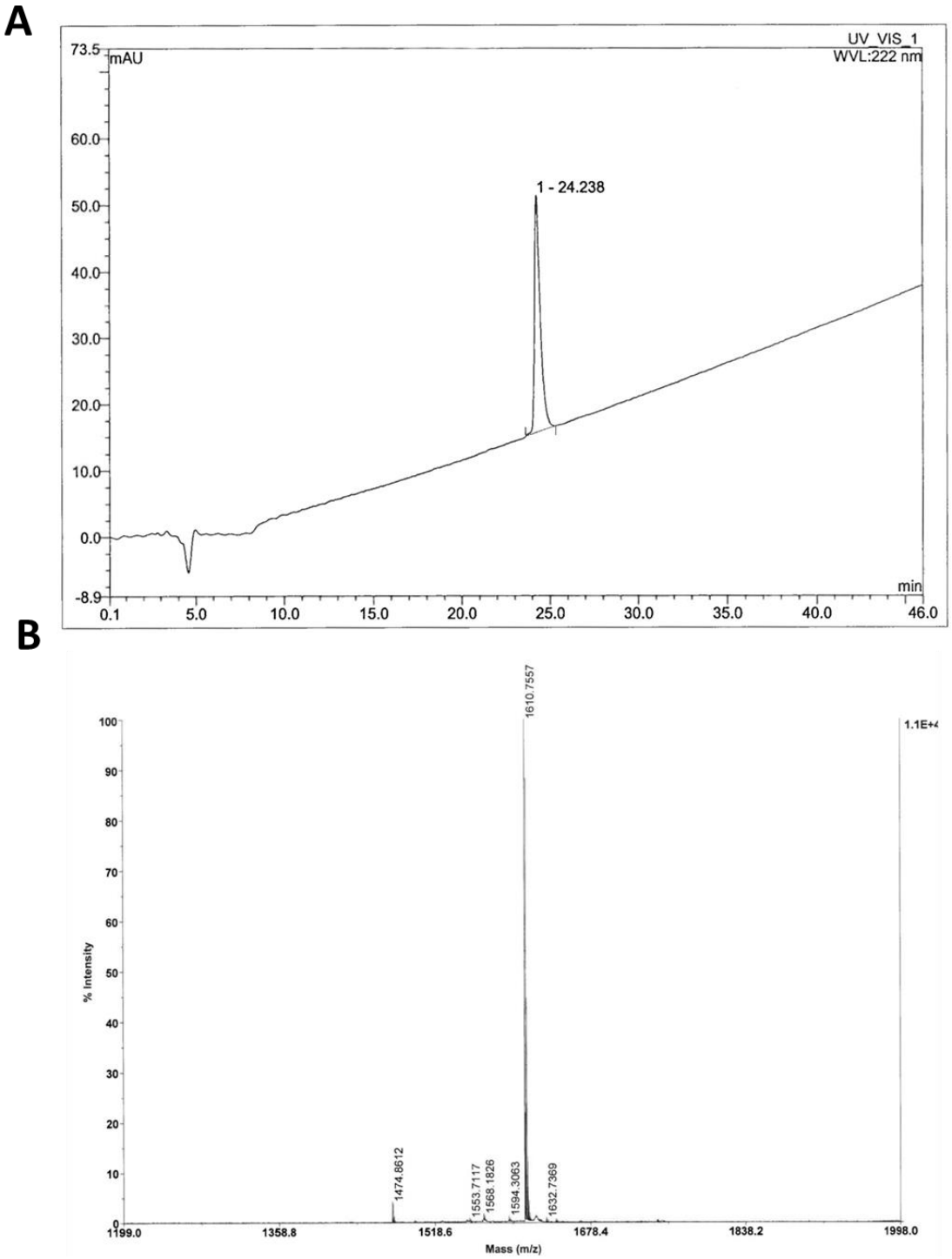

Supplemental Figure 5. (A) Analytical HPLC chromatogram and (B) MALDI-TOF of La-DOTA-MC1RL.

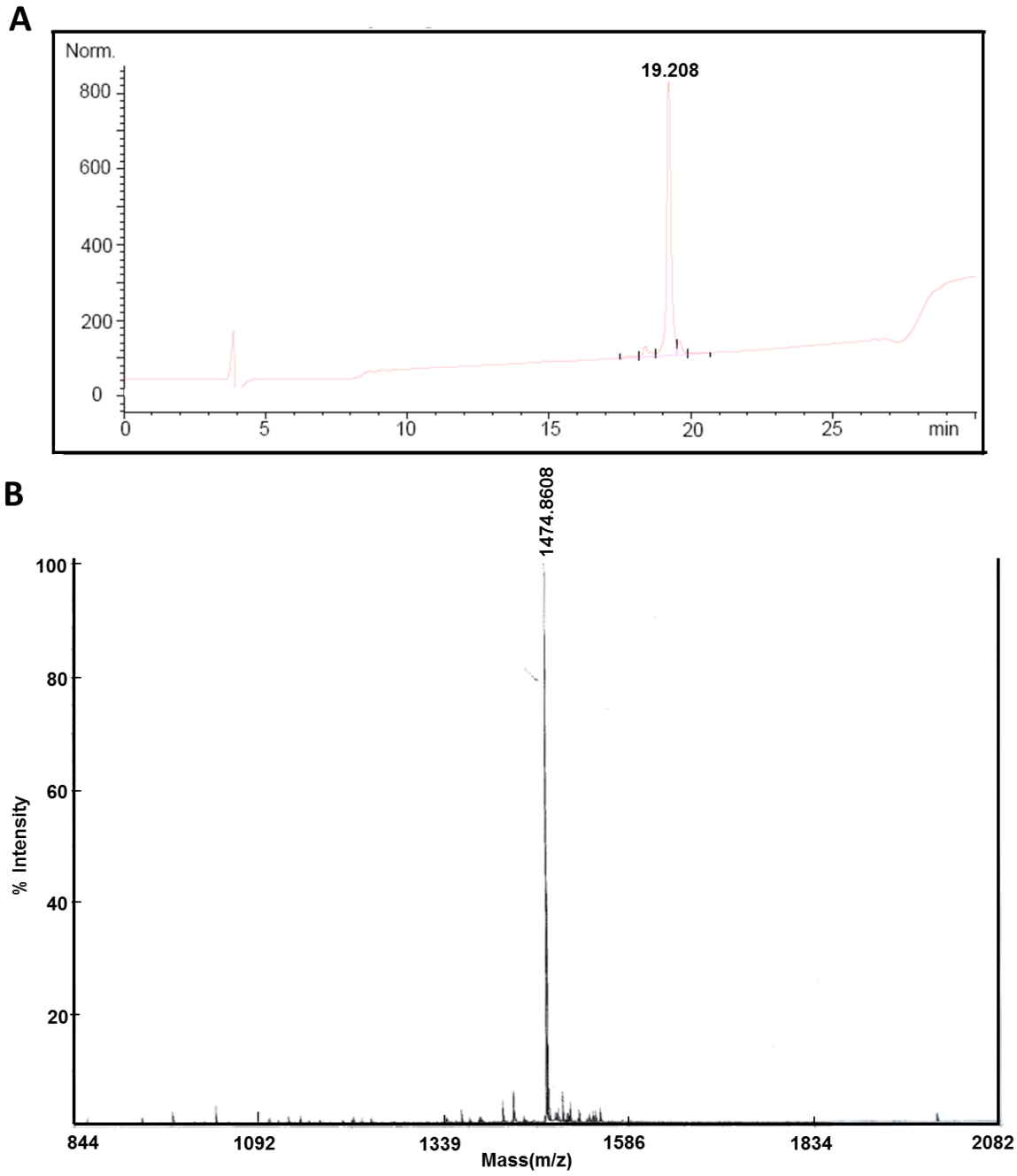

Supplemental Figure 6. (A) Analytical HPLC chromatogram and (B) MALDI-TOF of DOTA-SP (scrambled peptide).

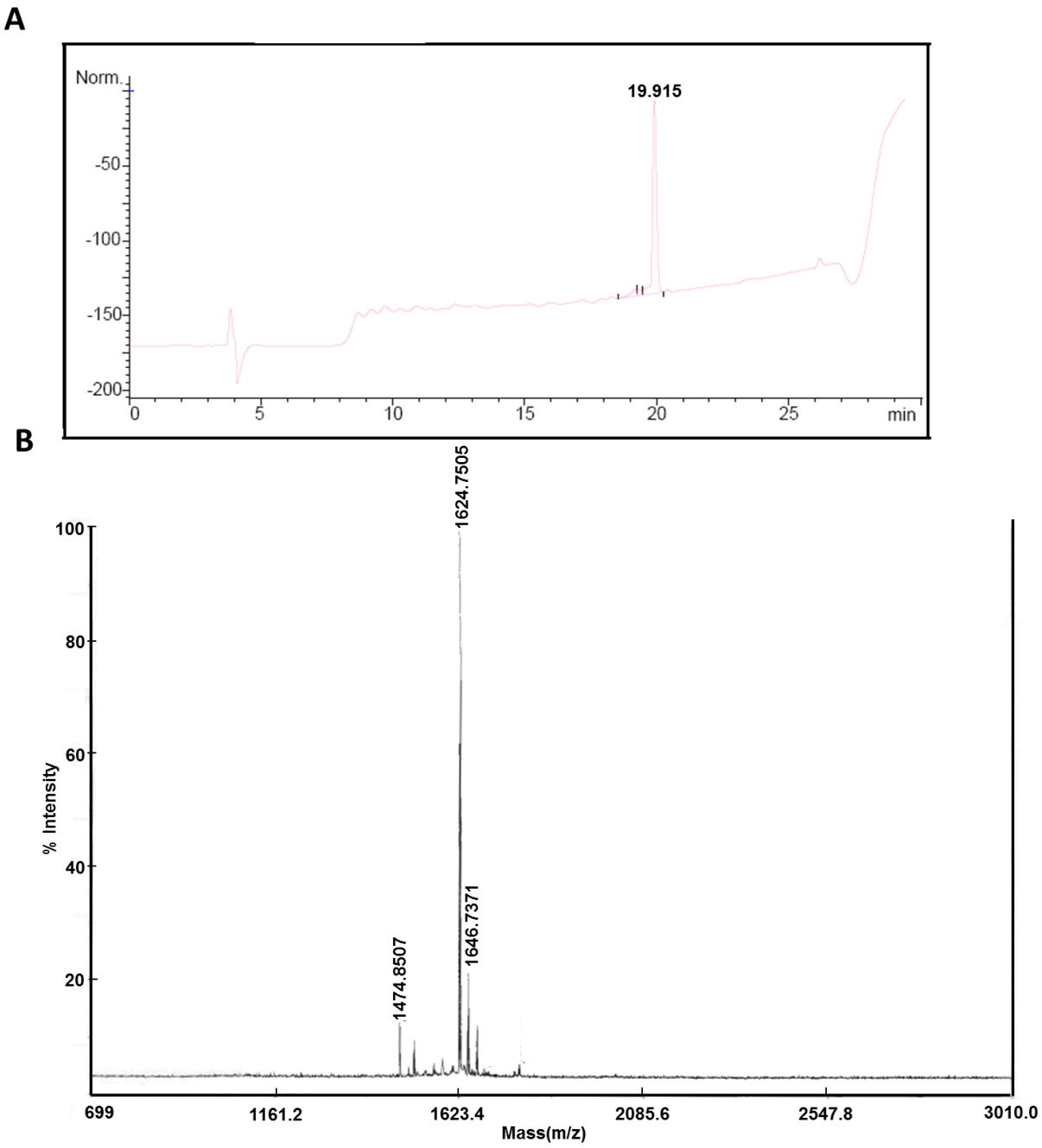

Supplemental Figure 7. (A) Analytical HPLC chromatogram and (B) MALDI-TOF of Eu-DOTA-SP.

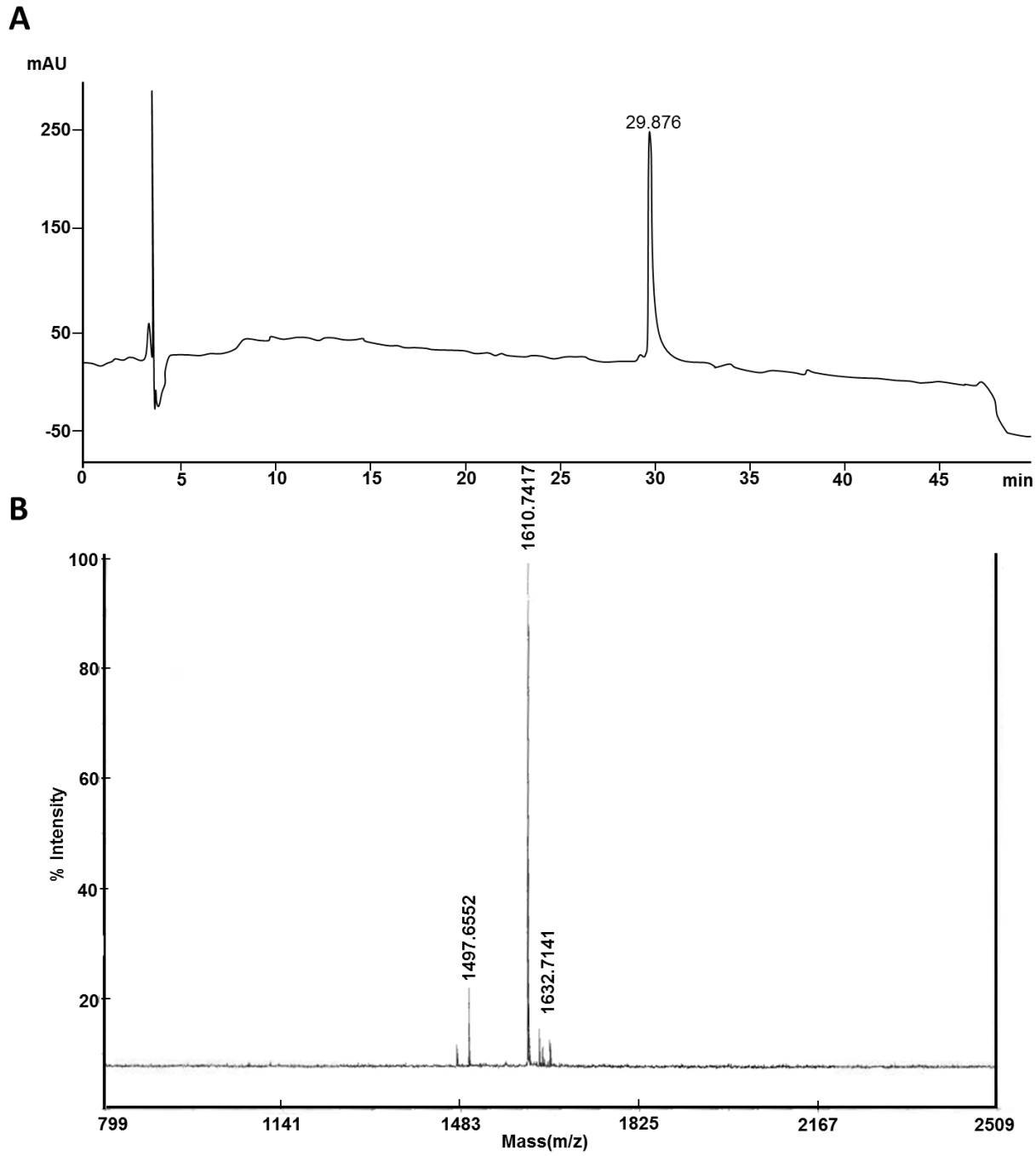

Supplemental Figure 8. (A) Analytical HPLC chromatogram and (B) MALDI-TOF of La-DOTA-SP.

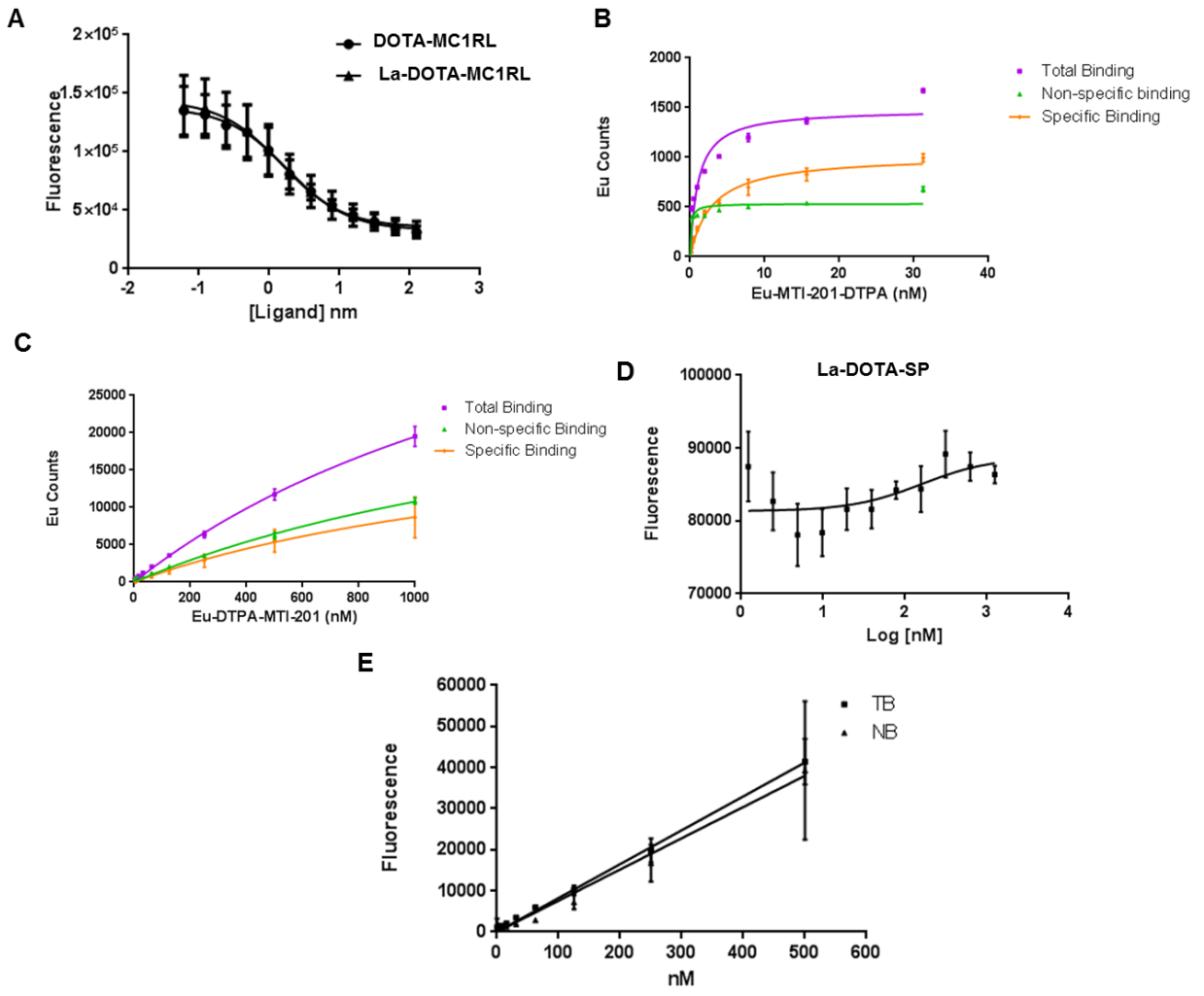

Supplemental Figure 9. Binding assay results. (A) Competitive binding assays of DOTA-MC1RL and La-DOTA-MC1RL conjugates. The binding affinities of DOTA-MC1RL (unlabeled) and La-DOTA-MC1RL were calculated to be 0.24 and 0.23 nM K_i, respectively. (B) Saturation binding assays to determine binding affinity of Eu-DTPA-MC1RL (4.4 nM K_d) using Hek293/MC1R (engineered cells to over-express MC1R) (C) Saturation binding assays to determine binding affinity of Eu-DTPA-MC1RL (1.3 µM K_d) to murine MC1R using the B16-F10 murine melanoma cell line. (D) Competitive binding assay of the La-DOTA-SP and (E) saturation binding assay of Eu-DOTA-SP . All assays used Hek293/MC1R cells (Hek293 cells that are engineered to overexpress MC1R).

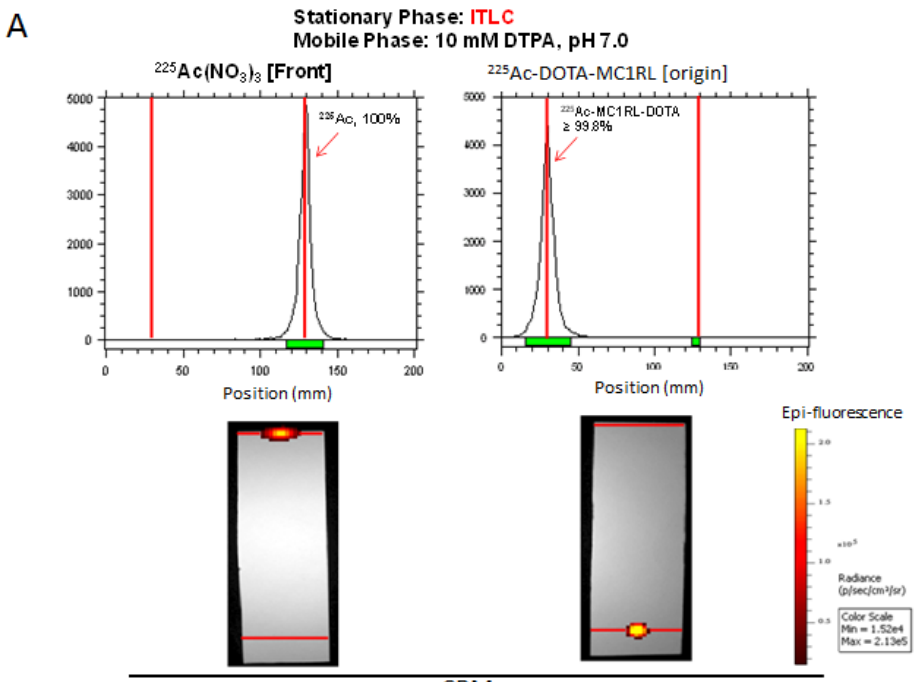

Radiotracer	CPM		Radiochemical Purity
	Origin	Front	
$^{225}Ac(NO_3)_3$	93.6	157816.5	100% (Front)
^{225}Ac-DOTA-MC1RL	157920.3	307.2	99.8% (Origin)

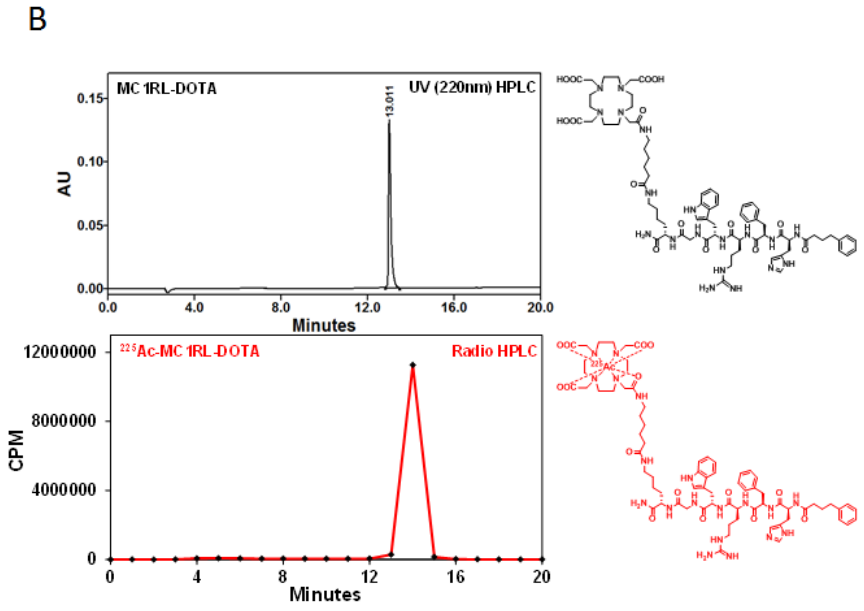

Supplemental Figure 10. Radiochemical purity of ^{225}Ac-DOTA-MC1RL. (A) Radio-TLC (top) and its corresponding Cherenkov luminescence imaging (middle) and quantification by gamma-counter (energy window = 150-500 keV, below). (B) Radio HPLC (radiolabeling yield: ≥95% and radiochemical purity: ≥99.8%).

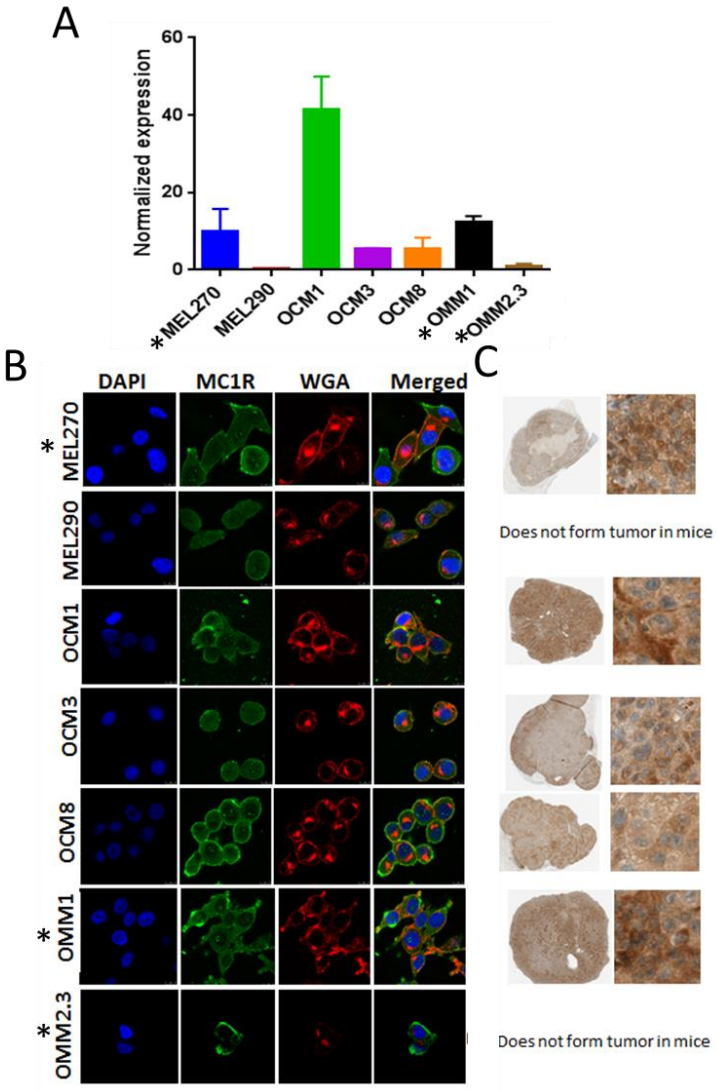

Supplemental Figure 11. MC1R expression in uveal melanoma cells: (A) mRNA, (B) Confocal micrographs of nuclear stain (blue), MC1R stain (green) and membrane stain (red). Co-localization of MC1R with membrane (yellow in merged image) indicates localization of MC1R on the cell-surface. (C) MC1R IHC staining of xenograft tumors from the same cell lines. *Cells with the GNAQ or GNA11 uveal melanoma mutations.

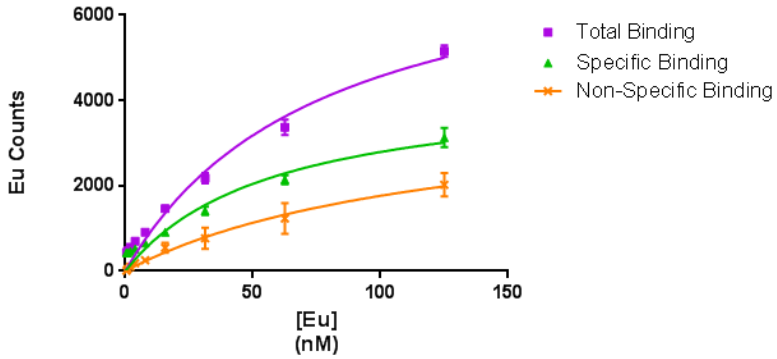

Supplemental Figure 12. Representative saturation binding assay for MEL270 cells. Saturation binding assays were performed using Eu-DTPA-MC1RL. Increasing amounts of Eu-DTPA-MC1RL were added to MEL270 cells. Binding specificity was determined in the presence of 5 μM unlabeled DOTA-MC1RL.

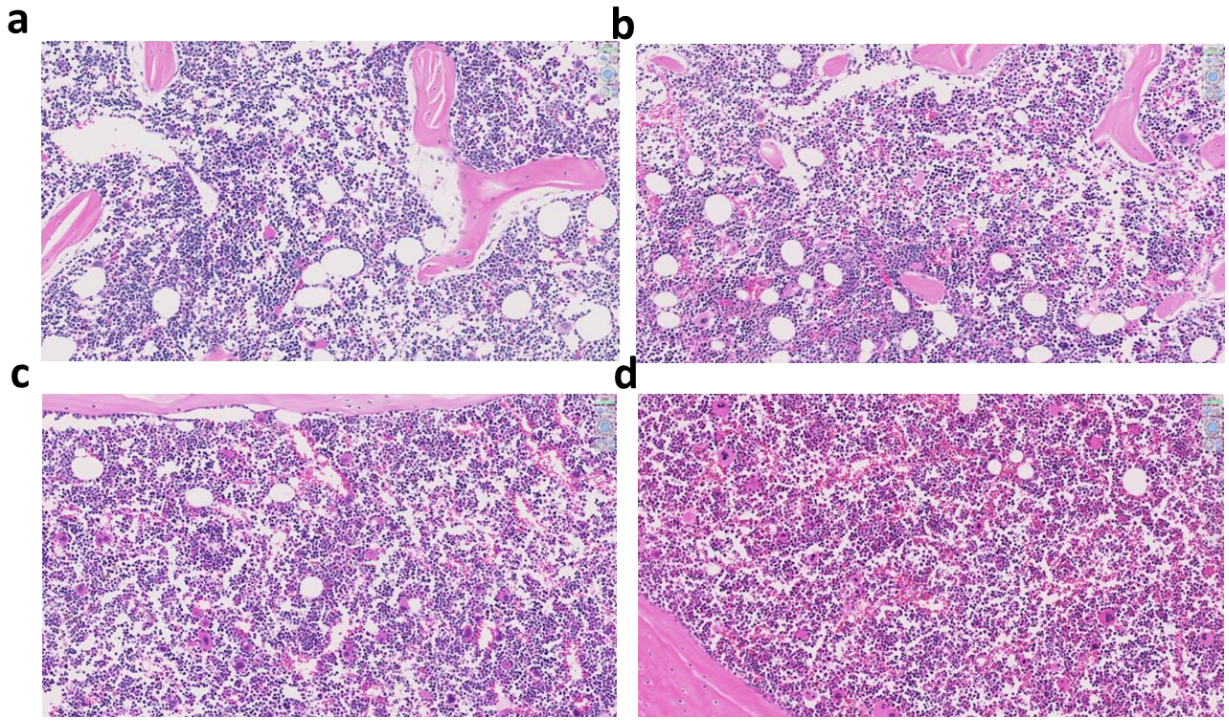

Supplemental Figure 13. Photomicrographs of mouse bone marrow (20X, H&E) 118 days post-injection. (a) Control (PBS), (b) 0.75 µCi (27.75 kBq), (c) 1 µCi (37 kBq) or (d) 4 µCi (148 kBq) of ^{225}Ac-DOTA-MC1RL. For all panels, the cellularity is within expected limits with adequate erythroid and myeloid precursors and maturation progression. The large multinucleated cells are normal megakaryocytes. The prominent clear spaces are venules/capillaries artifactually distended as a result of perfusion technique.

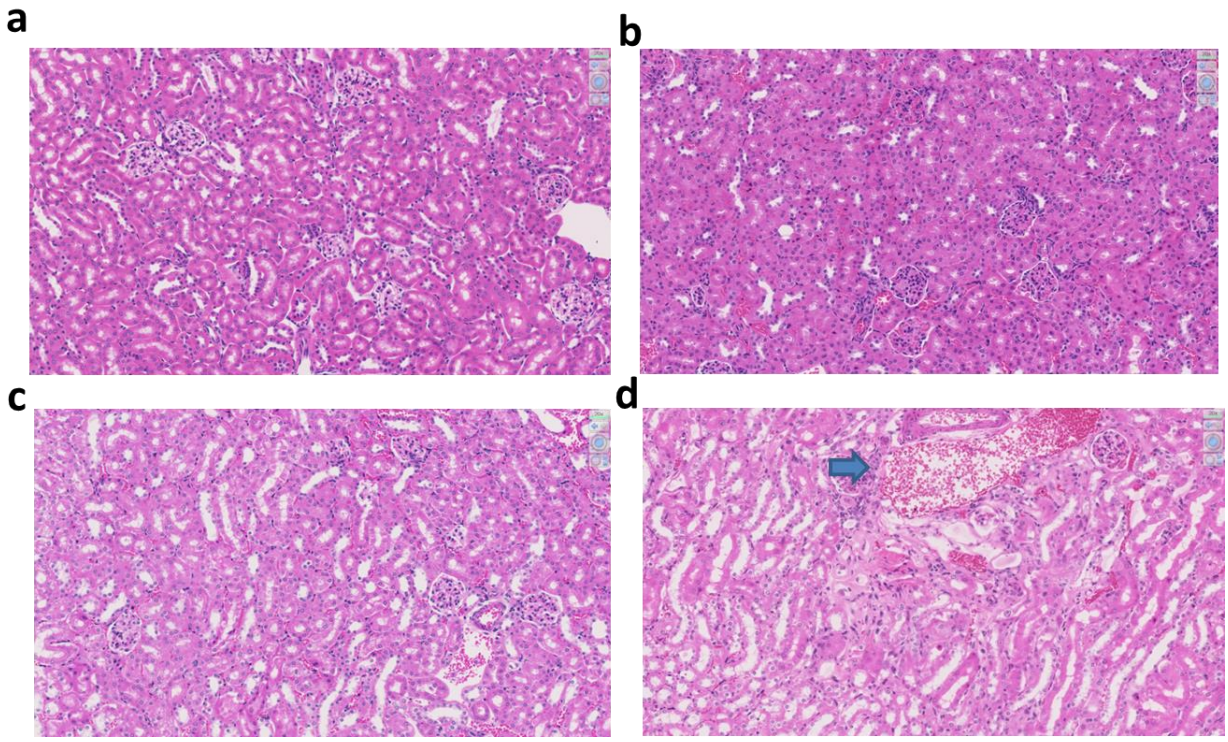

Supplemental Figure 14. Photomicrographs of mouse kidney (20X, H&E) 118 days post-injection. (a) Control (PBS), (b) 0.75 µCi (27.75 kBq), (c) 1 µCi (37 kBq) or (d) 4 µCi (148 kBq) of ^{225}Ac-DOTA-MC1RL. (a) & (b) The tissue is within normal limits, without disruption of the parenchyma, uniform tubules, and normal glomeruli. (c) Portions of the capsule are present along the top of the image with the cortex and adjacent corticomedullary junction present below. The tissue is within normal limits, with uniform tubules, and normal glomeruli. (d) A focus of fibrosis in the interstitium in the center of the field distorts the architecture and appears to sequester the tubules. A blood-filled vessel is indicated by the blue arrow. The tubular epithelium is attenuated (thinned) and reduced in number in this area (indicative of tissue injury with attempted healing).

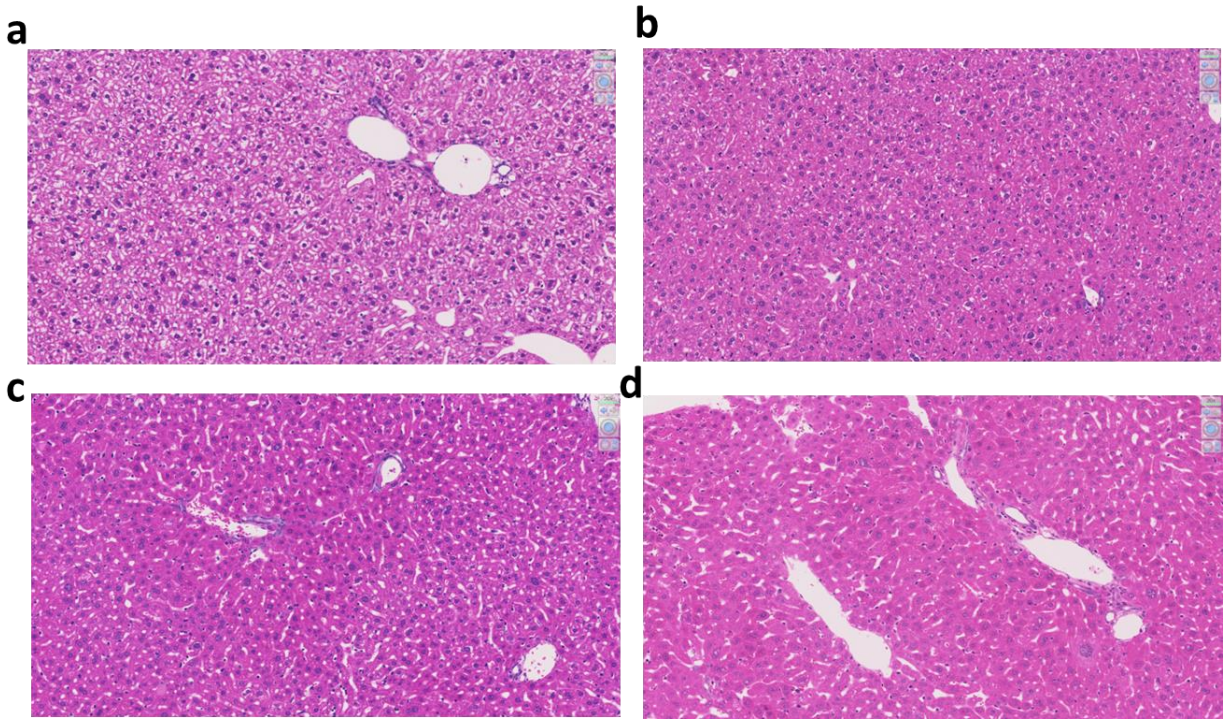

Supplemental Figure 15. Photomicrographs of mouse liver (20X, H&E) 118 days post-injection. (a) Control (PBS), (b) 0.75 µCi (27.75 kBq), (c) 1 µCi (37 kBq) or (d) 4 µCi (148 kBq) of ^{225}Ac-DOTA-MC1RL. For all panels, the hepatic architecture is within normal limits. The apparent 'laciness' of the hepatocyte cytoplasm is due to the presence of gylcogen and is a physiologic, not pathologic change. Glycogen is produced and stored in the liver. The prominence of the sinusoids and vessels is an artifact of the perfusion technique. The variation in hepatocyte nuclear size is normal in mice. (d) A portal triad is visible on the right side of the image with a portal vein, artery and bile duct. A central vein is present on the left side of the image.

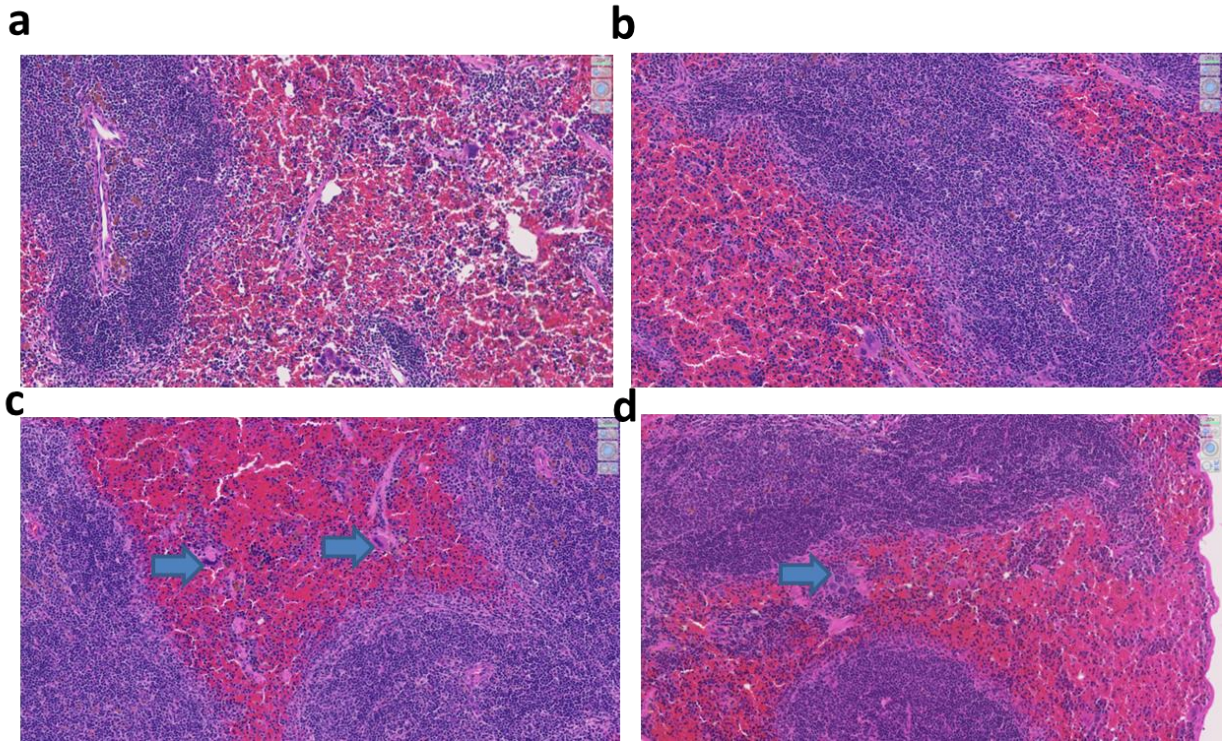

Supplemental Figure 16. Photomicrographs of mouse spleen (20X, H&E) 118 days post-injection. (a) Control (PBS), (b) 0.75 µCi (27.75 kBq), (c) 1 µCi (37 kBq) or (d) 4 µCi (148 kBq) of ^{225}Ac-DOTA-MC1RL. Normal megakaryocytes are present in the red pulp, (a,b) in the middle at the bottom edge of the image and (c,d) at the arrows, that are indicative of extramedullary hematopoiesis, which is normal in rodent spleen. Lymphocytes are adequately abundant in the white pulp, on the (a) left, (b) middle bottom, (c) either side and (d) top and bottom of the images. The prominence of the sinusoids and vessels is an artifact of the perfusion technique. (a) Brown pigment is evident and reflects iron stores within marcophages, normal in the spleen.

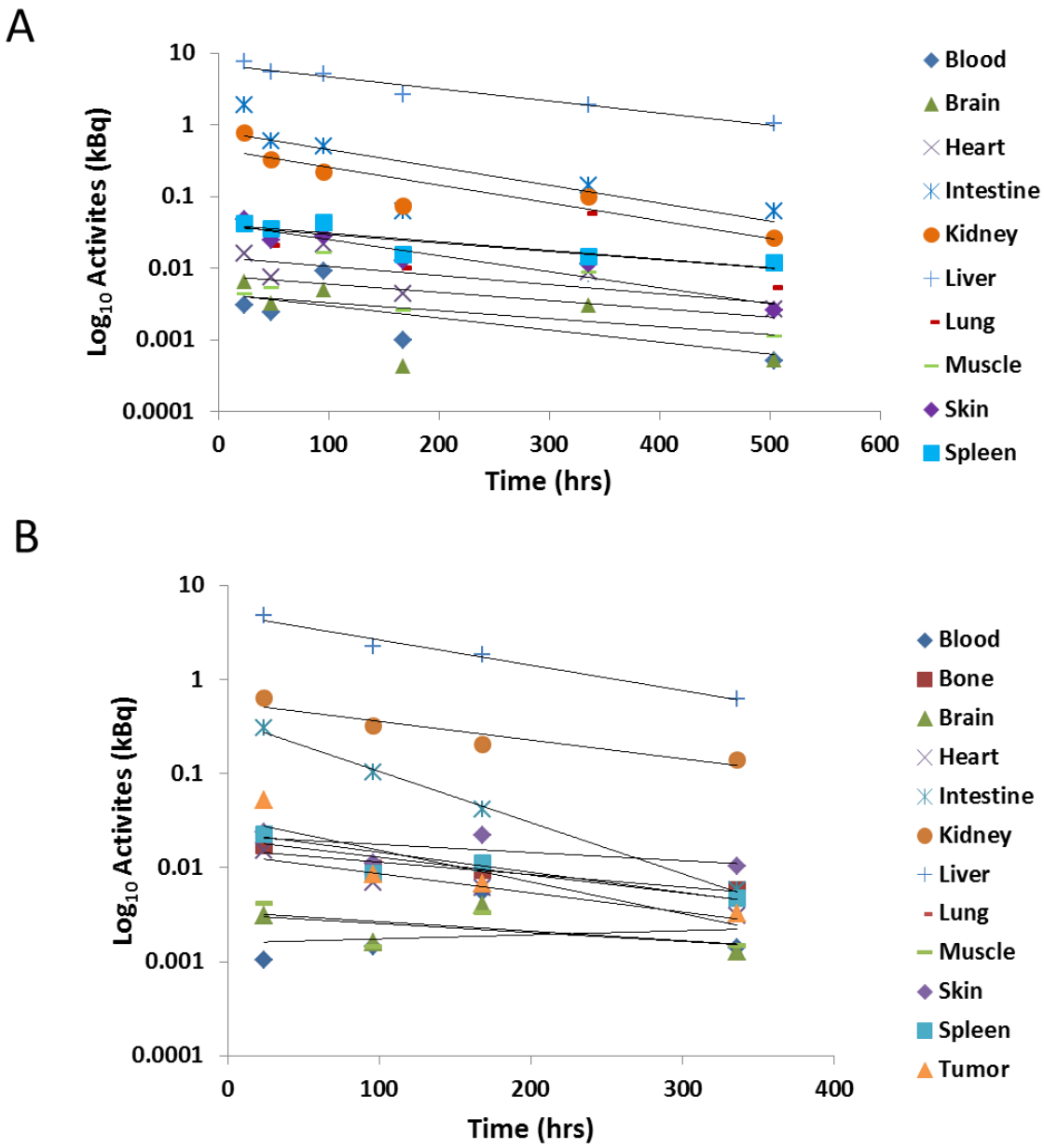

Supplemental Figure 17. Graphs of ^{225}Ac activities in select tissues over time and corresponding exponential line fits following administration of ^{225}Ac-DOTA-MC1RL: (A) Non-tumor bearing BALB/c mice and (B) SCID mice bearing MEL270 human uveal melanoma tumors.

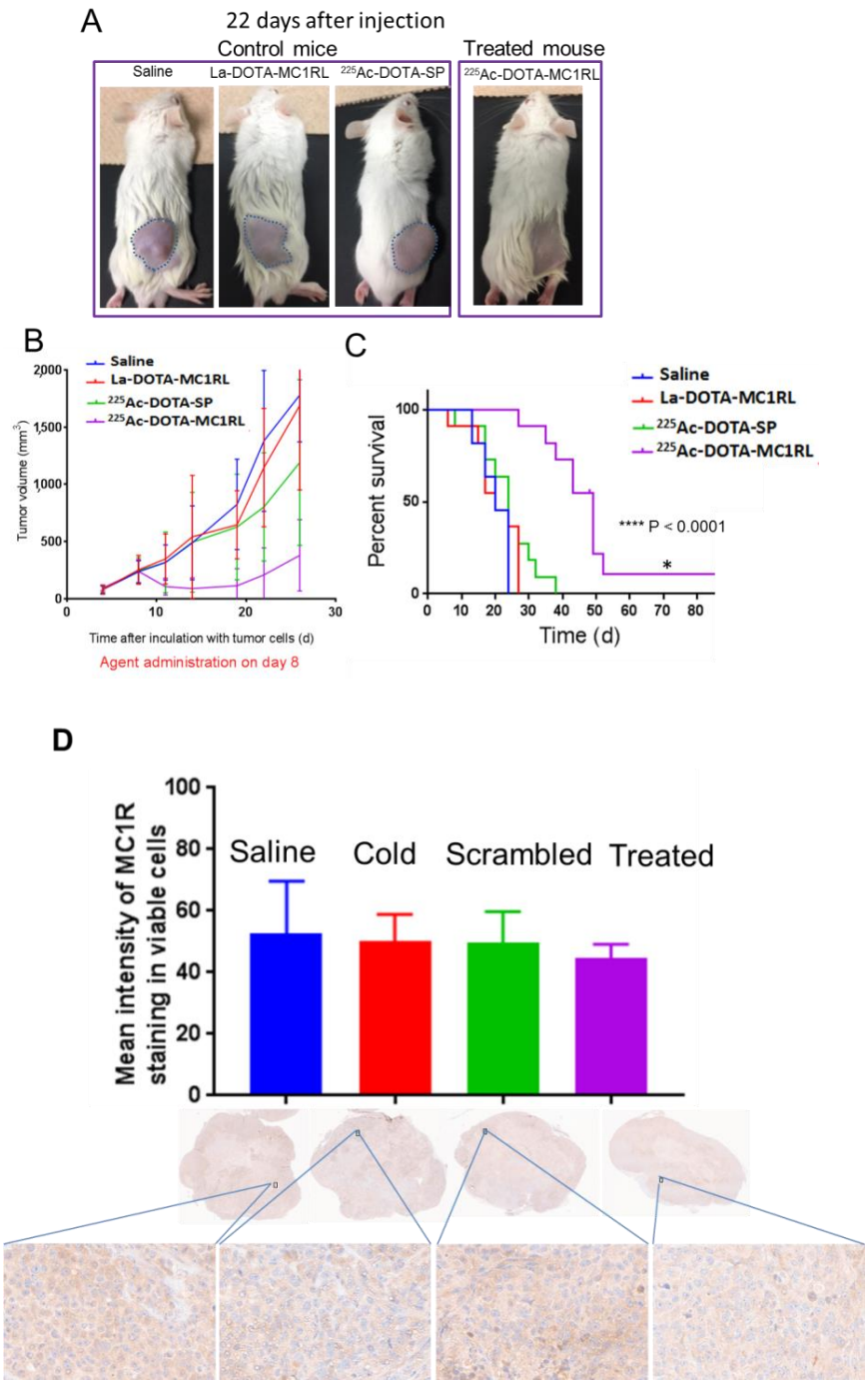

Supplemental Figure 18. Efficacy study in mice bearing A375/MC1R tumors: (A) Representative images of tumors (outlined); (B) initial tumor growth volumes; and (C) Kaplan-Meier plots. (D) MC1R staining of A375/MC1R tumors after reaching endpoints.

*One mouse in the ^{225}Ac-DOTA-MC1RL group died on day 49 due to an undeterminable cause but another lived cancer-free until 315 days p.i. and died of natural causes without any sign of cancer as determined by necropsy.